Analytical investigation of correlated charge collection in CCDs

Preprint typeset in JINST style - HYPER VERSION

Analytical Investigation of Correlated Charge Collection in CCDs

D. P. Weatherill[a*], K. D. Stefanov[a], A. D. Holland[a] and D. Jordan[b]

[a] *Centre for Electronic Imaging,*
The Open University, Walton Hall, Milton Keynes MK76AA, UK
E-mail: daniel.weatherill@open.ac.uk
[b] *e2v Technologies Ltd,*
106 Waterhouse Lane, Chelmsford CM1 2QU, UK

ABSTRACT: Correlated charge collection phenomena in CCD sensors are presently of interest due to their potentially major implications in space and ground based astronomy missions. These effects may manifest as a signal dependent Point Spread Function (PSF), or as a nonlinearity in the Photon Transfer Curve (PTC). We present the theoretical background to a simple analytical model based on previously published solutions of Poisson's equation which aims to aid conceptual understanding of how various device parameters relate to the magnitude of correlated charge collection. We separate correlated charge collection into two components - firstly excess diffusion caused by increasing drift time as the electric field in the device decreases, which is isotropic, and secondly anisotropic pixel boundary shifting as the fringing field in the parallel transfer direction collapses. Equations are presented which can be solved numerically to give reasonable detail, or solved analytically using simplifying approximations.

KEYWORDS: Correlated Charge Collection; CCD; Brighter Fatter Effect; deep depletion.

*Corresponding author.

Contents

1. Introduction

In recent years, signal dependent charge collection processes in thick CCDs have been reported [1]. The effect may be observed as a nonlinearity in the mean vs. variance curve (even though the illumination level vs. mean curve is linear), or as a broadening of the detector Point Spread Function (PSF) [2]. This broadening is generally observed to be larger in the parallel transfer direction than the serial [3], which leads to a change in the apparent aspect ratio of point sources of different brightnesses. This phenomenon has important implications in, for example, weak lensing measurements [4] and for deep astronomical surveys [5].

Autocorrelation analysis on flat fielded images [1] showed that the effect was due to a correlation in signal levels between nearby pixels - those pixels which contain more signal become less likely to accumulate further signal. In the flat field case, the initial variations among pixels arise due to the shot noise of the incident illumination. Therefore, correlated charge collection ultimately results in the variance of the pixel signals being lower than that expected by Poisson statistics (and thus to the nonlinearity of the photon transfer curve). If the incident illumination is a point source, then large variations in pixel signal levels result from the spatial distribution of the beam; thus correlation effects lead to the broadening of the PSF, as surrounding (dimly illuminated) pixels gather more of the charge that was intended to illuminate the central (bright) pixel.

Much progress has been made towards documenting and explaining correlated charge collection. Statistical models have been developed by Stefanov [6], which show that only very simple correlation relationships are needed between nearest neighbour pixels to reproduce qualitatively the form of the photon transfer curves (PTC) observed. Unfortunately, these models in themselves do not provide much physically motivated explanation or predictive power. By considering simple cases of disruption of the drift field lines caused by collected charges, Antilogus et al. [3]

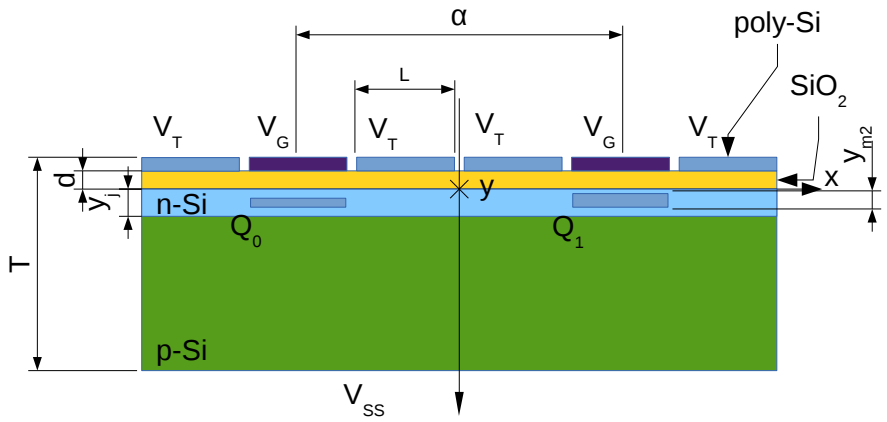

Figure 1. Device schematic, showing dimensions and potentials as listed in Table 1

constructed a model which gave basic agreement with both the PTC and the PSF broadening. Rasmussen [7] developed a framework where these drift field changes are regarded as, in effect, causing pixel boundaries to become dynamic. This approach is extremely successful in both conceptual and quantitative explanation. The dynamic pixel boundary approach can be used to obtain auxilliary pixel information which can in turn be used to correct for correlated charge collection.

Our motivation is to provide a simple approach which can help in examining dynamic pixel boundaries. We aim to avoid reliance on complex finite element approaches, and give physically motivated analytical expressions which, whilst approximate, may be of use in areas where minimum computation time is of value (e.g. realtime detector simulation) and in visualising basic relationships between detector geometry, bias conditions and charge correlation effects.

2. Analytical Charge Collection Models

We limit our consideration to thick, fully depleted devices where any diffusion effects due to a field free region may be disregarded. We also assume that the electronic diffusivity and mobility are constant and isotropic.

Two contributions to correlated charge collection are identified and investigated: the excess outward diffusion caused by an increase in the drift time for collected carriers as the electric field decreases with increasing stored charge (which is isotropic in the serial and parallel space directions), and the shift in pixel boundaries caused by changes in the fringing fields - which affects principally the parallel transfer direction. These two effects will interact with each other, introducing further complication, though this is not considered here.

In the following discussion, all potentials are referenced to the substrate potential, which is taken to be $V_{SS} = 0$. All numerical results are given for a fictitious device with parameters as given in Table 1, and geometry as shown in Figure 1. The depletion layer approximation is used, and the space charge distribution within the device is taken as constant density rectangular blocks.

Table 1. Device parameter values

Parameter Name	Symbol	Value
Buried Channel Donor Concentration	N_D	$1\times10^{16}\,\mathrm{cm}^{-3}$
Bulk Acceptor Concentration	N_A	$5\times10^{12}\,\mathrm{cm}^{-3}$
Junction Depth	y_j	$1.0\,\mu\mathrm{m}$
Oxide thickness	d	$0.1\,\mu\mathrm{m}$
Collecting Gate Voltage	V_G	$45V$
Low Gate Voltage	V_T	$30V$
Collecting Gate Width	L	$5\,\mu\mathrm{m}$
Device Thickness	T	$100\,\mu\mathrm{m}$
Mobility	μ	$1400\,\mathrm{cm}^2\,\mathrm{V}^{-1}\,\mathrm{s}^{-1}$
Diffusivity	D	$35\,\mathrm{cm}^2\,\mathrm{s}^{-1}$
Pixel Pitch	α	$15\,\mu\mathrm{m}$
Silicon Permittivity	ε_{si}	11.7
Oxide Permittivity	ε_{ox}	3.9

3. Excess Diffusion

We start from the 1D solution to Poisson's equation in an n-channel buried channel CCD as given by Yin and Cooper [8]. The potential ϕ at a depth y deeper than the charge storage depth y_{m2} is given by:

$$\phi(y) = \begin{cases} V_m - \frac{q\cdot N_D (y-y_{m2})^2}{2\cdot\varepsilon_{si}\cdot\varepsilon_0} + \phi_c(y) & y_{m2} < y < y_j \\ \frac{q\cdot N_A (y_p-y)^2}{2\varepsilon_{si}\cdot\varepsilon_0} + \phi_c(y) & y > y_j \end{cases} \tag{3.1}$$

where q is the elementary charge, and V_m is the channel potential, given by (eq. 5 from [8]):

$$V_m = \left(1+\frac{N_A}{N_D}\right)\left(V_G+V_1+V_2-\sqrt{V_2^2+2\cdot V_2\cdot(V_G+V_1)}\right) \tag{3.2}$$

$$\text{where}\, V_1 = \frac{q\cdot N_D\cdot y_t^2}{2\cdot\varepsilon_{si}\cdot\varepsilon_0}\left(1+\frac{2\cdot\varepsilon_{si}\cdot d}{\varepsilon_{ox}\cdot y_t}\right) \tag{3.3}$$

$$\text{and}\, V_2 = \frac{q\cdot N_A y_t^2}{2\cdot\varepsilon_{si}\cdot\varepsilon_0}\left(1+\frac{\varepsilon_{si}\cdot d}{\varepsilon_{ox}\cdot y_t}\right)^2 \tag{3.4}$$

where y_t is the charge adjusted junction depth:

$$y_t = y_j - \frac{Q}{q\cdot N_D} \tag{3.5}$$

with Q the charge stored in the channel. The "natural depletion depth", y_p, is given by:

$$y_p = y_j + \sqrt{\frac{2\varepsilon_{si}\cdot\varepsilon_0\cdot N_D\cdot V_m}{q\cdot N_A\cdot(N_A+N_D)}} \tag{3.6}$$

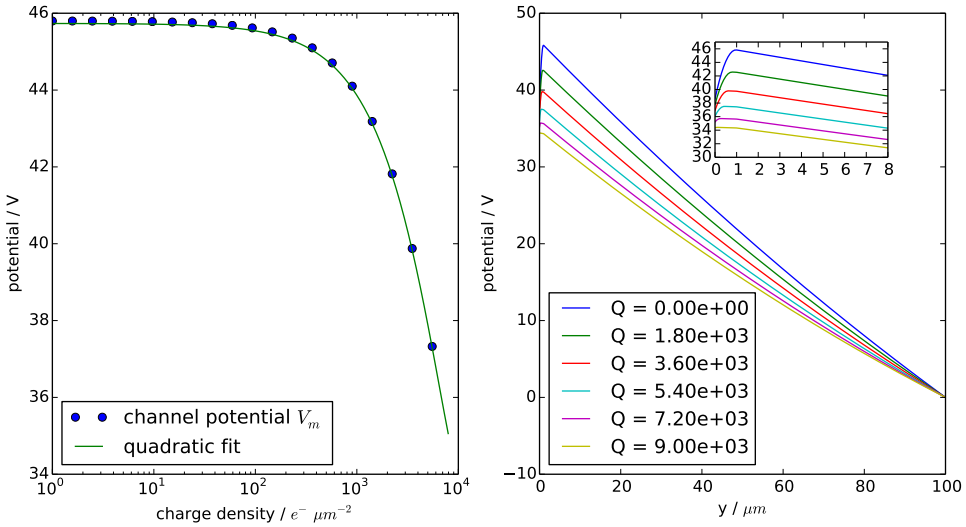

Figure 2. Illustration of the 1D analytical solution. Units of Q are $\mathrm{e}^{-}\mu\mathrm{m}^{-2}$

The compensating potential ϕ_c adjusts Yin and Cooper's solution for a fully depleted device of thickness T by making the solution satisfy the boundary condition $\phi(T) = 0$, and is given by:

$$\phi_c = \begin{cases} A \cdot (y+d) & -d < y < 0 \\ A\left(y \cdot \frac{\varepsilon_{ox}}{\varepsilon_{si}} + d\right) & y > 0 \end{cases} \tag{3.7}$$

$$\text{where } A = \frac{-q \cdot N_A \cdot (y_p - T)^2}{2 \cdot \varepsilon_{si} \cdot \varepsilon_0 \cdot \left(T \cdot \frac{\varepsilon_{ox}}{\varepsilon_{si}} + d\right)} \tag{3.8}$$

Resulting relationships between depth and potential, and channel charge and potential are shown in Figure 2

The electric field E can be obtained through differentiation:

$$E(y) = \begin{cases} \frac{q \cdot N_D \cdot (y - y_{m2}) - \frac{A}{\varepsilon_{ox}}}{\varepsilon_{si} \cdot \varepsilon_0} & y_{m2} < y < y_j \\ \frac{q \cdot N_A \cdot (y_p - y) - \frac{A}{\varepsilon_{ox}}}{\varepsilon_{si} \cdot \varepsilon_0} & y_j < y \end{cases} \tag{3.9}$$

and we then approximate (for now ignoring the 3D structure of the field lines) the drift time t_d for an electron starting at depth y_0 by:

$$\begin{aligned} t_d &= \int_{y_0}^{y_{m2}} \frac{dy}{-\mu \cdot E(y)} = \frac{\varepsilon_{si} \cdot \varepsilon_0}{q \cdot \mu} \left(\frac{1}{N_A} \cdot \int_{y_0}^{y_j} \frac{dy}{y - y_p + \frac{A}{\varepsilon_{ox}}} + \frac{1}{N_D} \cdot \int_{y_j}^{y_{m2}} \frac{dy}{y_{m2} - y + \frac{A}{\varepsilon_{ox}}} \right) \\ \Rightarrow t_d &= \frac{\varepsilon_{si} \cdot \varepsilon_0}{q \cdot \mu} \left(\frac{1}{N_A} \cdot \ln \left| \frac{y_p + \frac{A}{\varepsilon_{ox}} - y_j}{y_p + \frac{A}{\varepsilon_{ox}} - y_0} \right| + \frac{1}{N_D} \cdot \ln \left| \frac{y_j - y_{m2} + \frac{A}{\varepsilon_{ox}}}{\frac{A}{\varepsilon_{ox}}} \right| \right) \end{aligned} \tag{3.10}$$

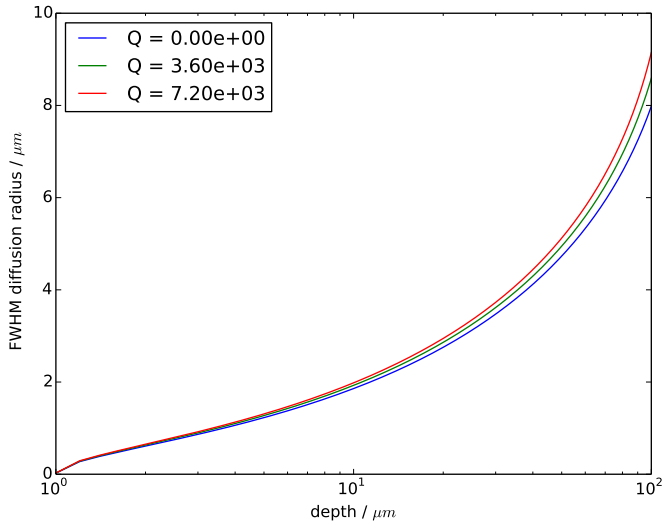

Figure 3. Excess diffusion radius of carriers at different depths caused by stored charge. Units of Q are $e^{-}\mu m^{-2}$

Note that stored charge dependences are introduced by the charge storage depth y_{m2}, the constant A and the natural depletion y_p. y_{m2} is given by ([8] eq. 10) :

$$y_{m2} = y_j - \sqrt{\frac{2 \cdot \varepsilon_s \cdot \varepsilon_0 \cdot N_A \cdot V_m}{q \cdot N_D \left(N_A + N_D\right)}} \tag{3.11}$$

the channel potential V_m being dependent on Q (see eq 3.2). Since typically, $N_D \gg N_A$ and $(y_j - y_{m2}) \ll (y_p - y_j)$, eq 3.10 implies that the diffusion effect near the channel is extremely small in this analysis[1]. More pertinently, since V_m decreases with increasing channel charge Q, this effect is actually in the opposite direction to that required for the observed effect: since the storage depth increases with extra charge, the drift time as the electron passes from the junction depth to the storage depth actually reduces. On the other hand, within the constant A, charge dependance appears as the factor $(y_p - T)^2$ (see eq 3.8). V_m decreases with increasing Q, so that y_p decreases (see eq 3.6), and hence the first term in eq 3.10 gives an increased drift time with increasing stored charge. The drift time variations are illustrated by Figure 3. This extra drift time corresponds to an increase in lateral diffusion (and hence charge sharing probability) of $\sim \sqrt{4 \cdot D \cdot t_d}$. Particular charges in two adjacent pixels may of course be diffusing in opposite directions, so that the average total contribution to observed correlation will depend on the difference between the two pixel charges. For a detailed example of the usage of this model in the flat field illumination case, see Appendix A.

4. Dynamic Pixel Boundaries

To approach an analytical analysis of dynamic pixel boundaries, a 2D solution of the Poisson equation incorporating stored charge is needed. We start from the elegant solution due to Lester and

[1] For typical values, this term is roughly 1×10^{-4} times smaller than the dominant contribution

Pulfrey [9]. The 2D potential in the device $\phi(x,y)$ is written as the sum of a homogeneous component $\phi_h(x,y)$, which is the solution neglecting space charge but satisfying the potential boundary condition at the gates, and a particular solution $\phi_p(x,y)$ which solves for the source term, with all the boundary conditions being set to zero.

$$\phi(x,y) = \phi_h(x,y) + \phi_p(x,y) \tag{4.1}$$

We incorporate stored charge into the model as follows: approximating the width of the stored charge packet in the x direction as equal to the width of the gate, we work out the potential at the junction depth under the collecting gates V'_G and under the non-collecting gates V'_T using the previously described 1D model. Then, repositioning the origin of our coordinates in the y direction such that $y' = y - y_j$, we solve the Poisson equation with the following boundary conditions:

$$V(x,0) = \begin{cases} V'_G & |x| > L/2 \\ V'_T & |x| < L/2 \end{cases}$$

where L is the collecting gate width (see Figure 1). The potential for a single pixel is, as given by [9]:

$$\begin{aligned} \phi_h(x,y') &= V'_T + \frac{V'_G - V'_T}{\pi} \cdot \left(\tan^{-1}\left(\frac{y'}{x - \frac{L}{2}} \right) - \tan^{-1}\left(\frac{y'}{x + \frac{L}{2}} \right) \right) \\ \phi_p(x,y') &= \frac{q \cdot N_A}{\varepsilon_{si} \cdot \varepsilon_0} \left(y' - \frac{(y')^2 - T^2}{2} \right) \end{aligned} \tag{4.2}$$

This simple expression conceals the complexity of the p-n junction, which is now part of the boundary conditions. Thus, it is inappropriate to use this expression to calculate potentials or fields shallower than the junction depth.

Since the mean free path of electrons in silicon is short, and neglecting diffusion, we can regard the streamlines of the Electric Field (see Figure 4) as electron trajectories. Whether an electron is captured in one pixel or another is determined by the zero contour of the electric field in the transfer direction, E_x. This can be calculated from eq. 4.2.

$$E_x(x,y') = -\frac{\partial \phi(x,y')}{\partial x} = \frac{V'_T + V'_G}{\pi} \left(\frac{y'}{\left(x + \frac{L}{2}\right)^2 + (y')^2} - \frac{y'}{\left(x - \frac{L}{2}\right)^2 + (y')^2} \right) \tag{4.3}$$

Note that there is no contribution from ϕ_p in eq. 4.3. [2]

Next we construct a two-pixel solution Λ_x, using the linearity of the Poisson equation:

$$\begin{aligned} \Lambda_x(x,y') = {} & \frac{V'_T +_1 V'_G}{\pi} \left(\frac{y'}{\left(\frac{L+\alpha}{2} + x\right)^2 + (y')^2} - \frac{y'}{\left(\frac{\alpha - L}{2} + x\right)^2 + (y')^2} \right) \\ & + \frac{V'_T +_2 V'_G}{\pi} \left(\frac{y'}{\left(\frac{L-\alpha}{2} + x\right)^2 + (y')^2} - \frac{y'}{\left(x - \left(\frac{L+\alpha}{2}\right)\right)^2 + (y')^2} \right) \end{aligned} \tag{4.4}$$

[2] In the case of a device lacking full depletion, ϕ_p now varies in both dimensions due to the depletion depth being a function of x. The field can still easily be found analytically, but subsequent solution of the zero contour will be much more difficult.

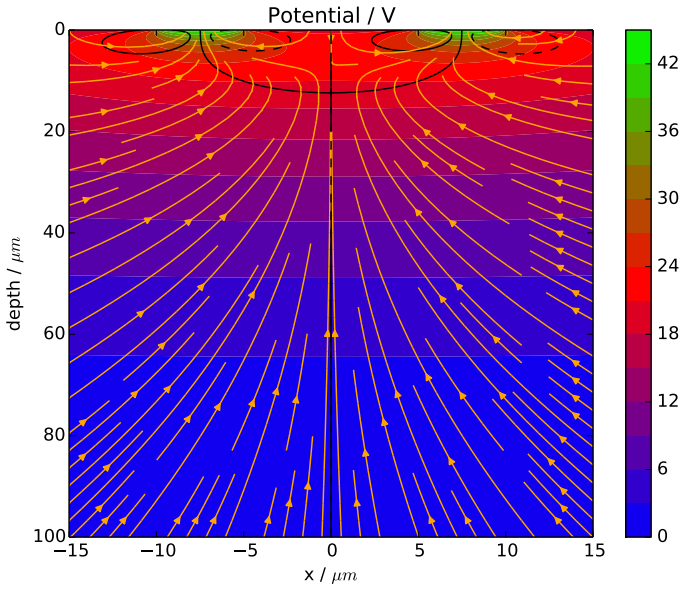

Figure 4. Potential contour plot of two neighbouring pixels. Orange arrows show electron trajectories, calculated from field streamlines. Solid black lines represent the zero field contours.

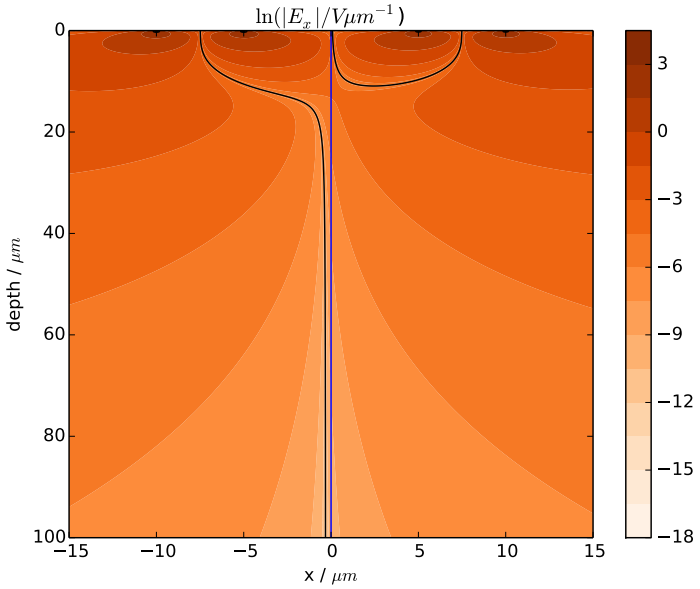

Figure 5. Example solution for the pixel boundary when $Q_0 > Q_1$. The boundary moves towards the pixel with more stored charge, reducing its effective area. Solid black lines represent the zero field contours.

where α is the distance between the centres of the two collecting gates, and ${}_1V'_G$ and ${}_2V'_G$ are the two junction potentials, which, being obtained from eq 3.1, depend on the stored channel charge. The equation $\Lambda_x = 0$ can be solved numerically (see Figure 5), or by taking y to be much

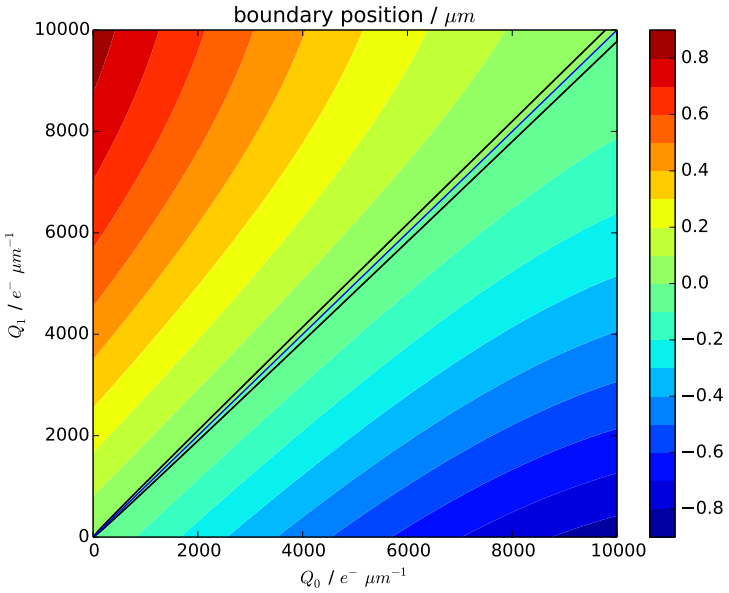

Figure 6. Effective pixel boundary position for deep interactions. The area between the black lines indicates the FWHM shot noise region.

larger than all other dimensions (i.e. deep interactions), the solution x_b can be obtained as:

$$x_b \approx \frac{\alpha}{2}\left(\frac{{}_1V'_G - {}_2V'_G}{V'_T + {}_2V'_G + {}_1V'_G}\right) \tag{4.5}$$

The relationship between V'_G and Q is well approximated by a quadratic fit (see Figure 2)

$$V'_G = \beta + \gamma \cdot Q + \delta \cdot Q^2 \tag{4.6}$$

And if the simplifying assumption is made that $Q_0 \approx Q_1 \approx \bar{Q}$ (valid, for example, in the flat field illumination case), and that $V'_T \approx \beta$, we can simplify eq 4.5 to:

$$x_b \approx \frac{\alpha}{2}\left(\frac{\left(\gamma + 2\cdot\delta\cdot\bar{Q}\right)\cdot\Delta Q}{3\cdot\beta + 2\cdot\bar{Q}\cdot\left(\gamma + \delta\cdot\bar{Q}\right)}\right) \tag{4.7}$$

where ΔQ is the difference between charges. This expression can be used as the starting point for Monte Carlo or approximate statistical simulations of experimental measurements such as PTCs and autocorrelation matrices. Alternatively, by solving eq 4.4 numerically, more detailed calculations can be performed giving the wavelength dependence of the boundaries. From Figure 6, it can be seen that for flat field illumination even the deep interactions (blue light in a back illuminated device), we expect that at around half the full well ($Q \sim 6000\,\mathrm{e}^-\,\mu\mathrm{m}^{-2}$), about half the pixels will experience a boundary shift of $\sim 20\,$nm or more, a correlation at around the 0.1% level. This is in reasonable agreement with recorded observation [6], when taken also with the larger isotropic component at the ~5% level.

5. Conclusions and Future Work

We have presented the underpinnings of a simple model which we hope can aid understanding of correlated charge collection effects in CCDs. Two components were considered, the isotropic excess diffusion caused by the reduction in the electric field perpendicular to the collecting gates, and the anisotropic component caused by a shift in the fringing field boundaries. Both of these parts warrant much further analytical investigation, and of course experimental testing. We have shown a simple, very naive example of calculating some real world numbers from the model (see Appendix A) , and much more work needs to be completed in this area before the approach may be labelled "robust". We soon hope to present verification of our model against both numerical finite element simulations, and laboratory data (using various thicknesses of the back illuminated e2v CCD-261 device).

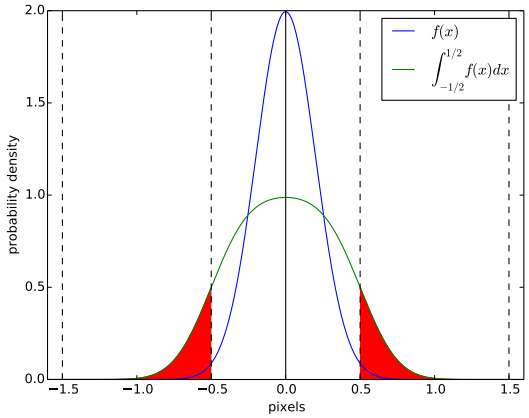

Figure 7. Illustration of a gaussian probability density function $f(x)$ used for flat field condition (blue line), and its integral (green line). The dashed lines represent pixel boundaries, and the red shaded region represents the value of the cumulative switching probability function, $\bar{g}(\sigma)$

A. Appendix: Calculation of Isotropic spreading under Flat Field Illumination

We begin by assuming that the charge generated in a δ-function like distribution within the device will diffuse in a Gaussian manner in 1D, resulting in a probability distribution for the electron positions x of

$$f(x) = \frac{1}{\sigma\sqrt{2\cdot\pi}} \cdot \exp\left(\frac{-x^2}{2\cdot\sigma^2}\right) \tag{A.1}$$

where σ is related to the drift time t_d and diffusivity D by $\sigma = \sqrt{4\cdot D\cdot t_d}$.

Flat field illumination is accounted for by integrating over the interval $[-\frac{1}{2},\frac{1}{2}]$ (working in pixel units throughout - see Figure 7). We integrate once more to find the cumulative distribution function, and then work out the total probability that an electron ends up outside the original pixel (for simplicity, we assume any electron outside the pixel it arrived in ends up in its nearest neighbour, and use only multiplicative factors to introduce 2D dependence):

$$g(\sigma) = \frac{1}{2} + \frac{\sqrt{2}\cdot\sigma}{2\cdot\sqrt{\pi}}\left(1-\exp\left(\frac{-1}{2\cdot\sigma^2}\right)\right) - \frac{1}{2}\cdot\mathrm{erf}\left(\frac{1}{\sqrt{2}\cdot\sigma}\right) \tag{A.2}$$

We can use the analysis in Section 3 (and particularly illustrated by Figure 3), to translate this drift time function $g(t_d)$ to an absorption depth and signal dependence, which is referred to as $\bar{g}(z,q)$, since the drift time is related to both of these quantities. For a back illuminated device, the probability density for a photon being absorbed at a depth z is:

$$p_{BI}(z) = \exp\left(\frac{-(T-z)}{z_0(\lambda)}\right) \tag{A.3}$$

and for a front illuminated device, simply:

$$p_{FI}(z) = \exp\left(\frac{-z}{z_0(\lambda)}\right) \tag{A.4}$$

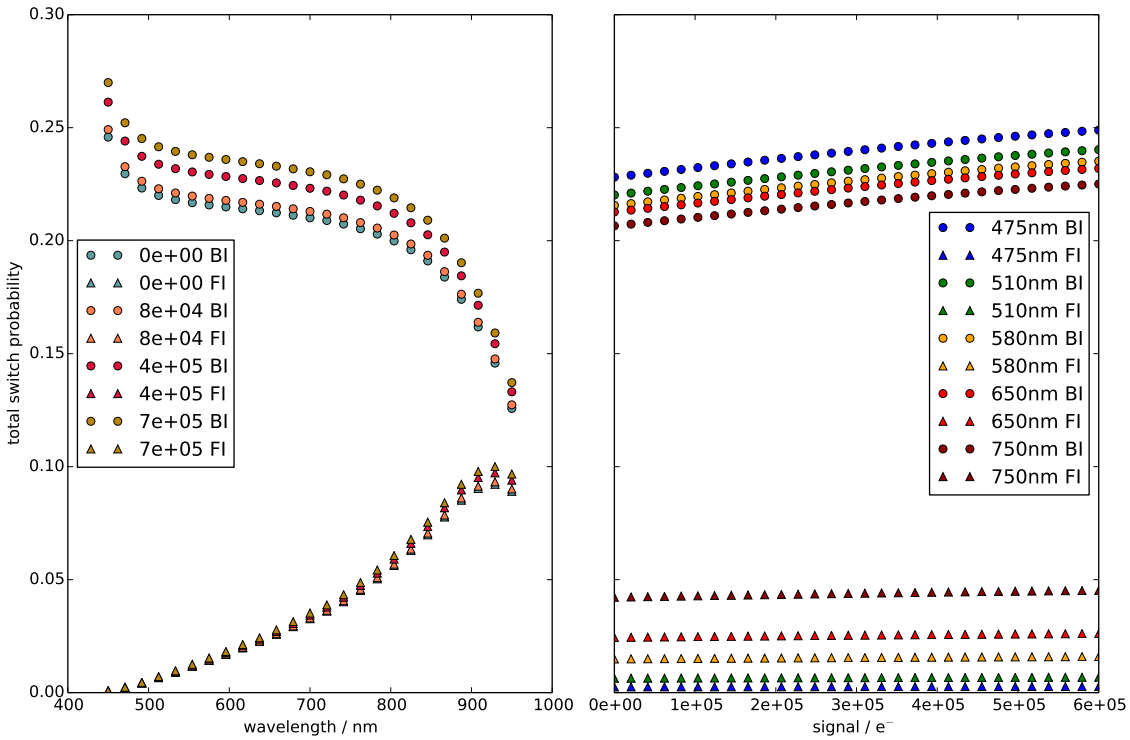

Figure 8. The calculated relationship between stored signal, wavelength and total switching probability. Front illuminated device behaviour is shown by triangles, Back illuminated by dots.

where $z_0(\lambda)$ is the absorption length in Si at wavelength λ [3], which is obtained from empirical data [10]. A weighted sum over all possible depths gives the total probability of an electron to be transferred to a surrounding pixel:

$$P(\lambda, q) = \int_0^T \exp\left(\frac{-(T-z)}{z_0(\lambda)}\right) \cdot \bar{g}(z,q) \cdot dz \tag{A.5}$$

which may be evaluated numerically. The results of this for both back and front illuminated cases are shown in Figure 8. Most of these transferred electrons are due to the static PSF of the device, and it is the excess signal dependent component which is of interest. To calculate the average signal per pixel that we expect to be moved "in excess" of the static PSF $\langle q \rangle_{\text{excess}}$, the following formula is used:

$$\langle q \rangle_{\text{excess}} = \int_0^q q' \cdot \frac{\partial P(\lambda, q')}{\partial q'} \cdot dq' \tag{A.6}$$

Somewhat simplistic estimates may then be made of correlation coefficients (by using the quantity $\langle q \rangle_{\text{excess}} / \langle q \rangle$). A photon transfer curve may also be approximated, by plotting mean signal $\langle q \rangle$ against $\langle q \rangle - \langle q \rangle^2_{\text{excess}}$. Both of these show qualitative agreement with published data (see Figure 9), the correlation coefficients being similar to those found by [11], and the relative magnitudes of the quadratic and linear coefficients of the fits to the photon transfer curve being similar to the data shown in [6].

[3] it should be noted that z_0 also varies with temperature[10], along with D, which we have not attempted to address

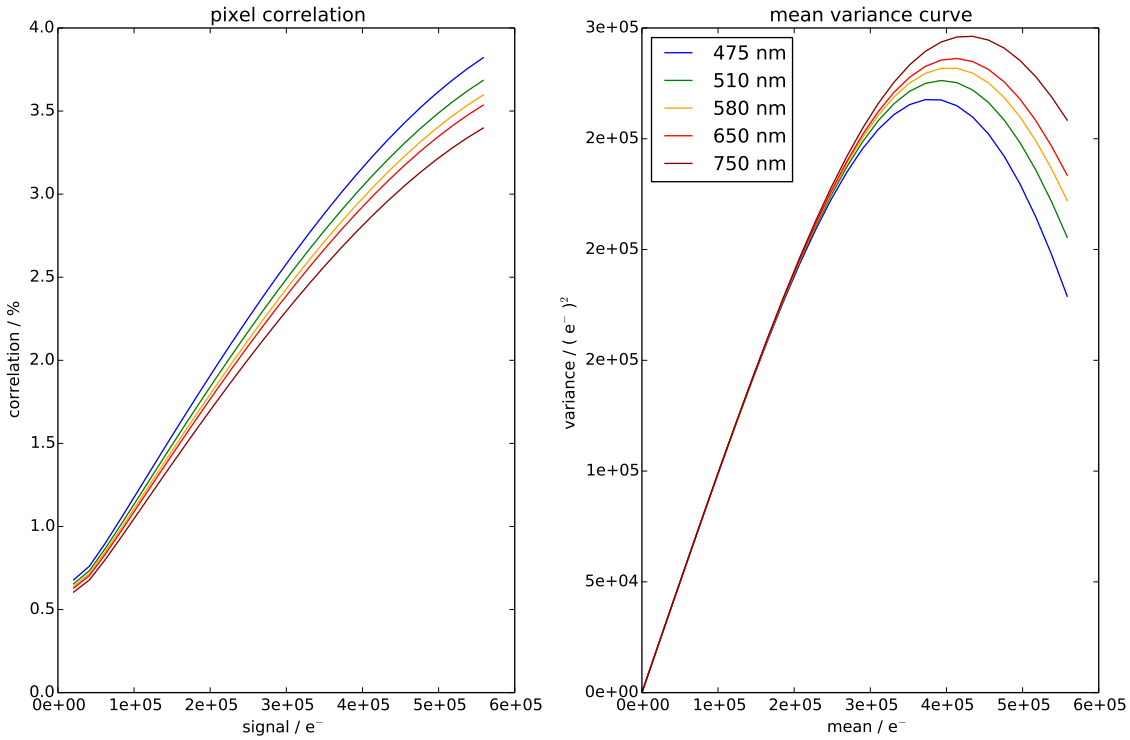

Figure 9. calculated results for correlation (left) and mean-variance (right) experiments at different wavelengths

References

[1] M. Downing, D. Baade, P. Sinclaire, S. Deiries, and F. Christen, *Ccd riddle: a) signal vs time: linear; b) signal vs variance: non-linear*, *Proc. SPIE* **6276** (2006) 627609–627609–11, [http://dx.doi.org/10.1117/12.671457].

[2] E. A. H. Allanwood, N. J. Murray, K. D. Stefanov, D. J. Burt, and A. D. Holland, *Point-spread function and photon transfer of a ccd for space-based astronomy*, *Proc. SPIE* **8860** (2013) 88600I–88600I–9, [http://dx.doi.org/10.1117/12.2024263].

[3] P. Antilogus, P. Astier, P. Doherty, A. Guyonnet, and N. Regnault, *The brighter-fatter effect and pixel correlations in ccd sensors*, *Journal of Instrumentation* **9** (2014), no. 03 C03048, [http://dx.doi.org/10.1088/1748-0221/9/03/C03048].

[4] R. Massey, H. Hoekstra, T. Kitching, J. Rhodes, M. Cropper, J. Amiaux, D. Harvey, Y. Mellier, M. Meneghetti, L. Miller, S. Paulin-Henriksson, S. Pires, R. Scaramella, and T. Schrabback, *Origins of weak lensing systematics, and requirements on future instrumentation (or knowledge of instrumentation)*, *Monthly Notices of the Royal Astronomical Society* (2012).

[5] J. A. Tyson, *Large synoptic survey telescope: Overview*, *Proc. SPIE* **4836** (2002) 10–20, [10.1117/12.456772].

[6] K. Stefanov, *A statistical model for signal-dependent charge sharing in image sensors*, *Electron Devices, IEEE Transactions on* **61** (Jan, 2014) 110–115, [http://dx.doi.org/10.1109/TED.2013.2291448].

[7] A. Rasmussen, *Pixel area variations in sensors: a novel framework for predicting pixel fidelity and distortion in flat field response*, *JINST* **9** (2014), no. 04 C04027, [arXiv:1403.3317].

[8] Y. Yin and J. Cooper, J.A, *Simple equations for the electrostatic potential in buried-channel mos devices*, *Electron Devices, IEEE Transactions on* **39** (Jul, 1992) 1770–1772, [http://dx.doi.org/10.1109/16.141247].

[9] T. P. Lester and D. Pulfrey, *A new method based on the superposition principle for the calculation of the two-dimensional potential in a buried-channel charge-coupled device*, *Electron Devices, IEEE Transactions on* **31** (Jul, 1984) 999–1001.

[10] K. Rajkanan, R. Singh, and J. Shewchun, *Absorption coefficient of silicon for solar cell calculations*, *Solid-State Electronics* **22** (1979), no. 9 793 – 795.

[11] M. Downing and P. Sinclaire, *The ccd riddle revisited: Signal vs time - linear, signal vs variance - non-linear*, *Scientific Detector Workshop* (2013).